coatings

MDPI

Review

Recent Advances in Graphene-Based Free-Standing Films for Thermal Management: Synthesis, Properties, and Applications

Feng Gong [1,*], Hao Li [1,†], Wenbin Wang [1,†], Dawei Xia [1], Qiming Liu [1], Dimitrios V. Papavassiliou [2,*] and Ziqiang Xu [1]

1 School of Materials and Energy, University of Electronic Science and Technology of China, Chengdu 611731, China; 15520768039m@sina.cn (H.L.); bingo_uestc@163.com (W.W.); davidxia97@163.com (D.X.); qimingliuwhr@gmail.com (Q.L.); nanterxu@uestc.edu.cn (Z.X.)

2 School of Chemical, Biological, and Materials Engineering, University of Oklahoma, Norman, OK 73019, USA

* Correspondence: gongfeng@uestc.edu.cn (F.G.); dvpapava@ou.edu (D.V.P.)

† These authors contributed equally to this work.

Received: 20 January 2018; Accepted: 4 February 2018; Published: 7 February 2018

Abstract: Thermal management in microelectronic devices has become a crucial issue as the devices are more and more integrated into micro-devices. Recently, free-standing graphene films (GFs) with outstanding thermal conductivity, superb mechanical strength, and low bulk density, have been regarded as promising materials for heat dissipation and for use as thermal interfacial materials in microelectronic devices. Recent studies on free-standing GFs obtained via various approaches are reviewed here. Special attention is paid to their synthesis method, thermal conductivity, and potential applications. In addition, the most important factors that affect the thermal conductivity are outlined and discussed. The scope is to provide a clear overview that researchers can adopt when fabricating GFs with improved thermal conductivity and a large area for industrial applications.

Keywords: graphene; free-standing films; thermal conductivity; thermal management

1. Introduction

Small yet powerful micro/nano-electronic devices used in electronic, portable, and automotive products generate a large amount of heat during operation, which may cause damage or failure [1–3]. There is a critical demand for methods and materials that can be used to dissipate the generated heat from microelectronic devices. As electronic devices become more and more miniaturized, this need is becoming more and more urgent. The current materials used for thermal dissipation in microelectronic devices are copper or aluminum alloys, which attain a thermal conductivity of 401 W/m·K and 121 W/m·K, respectively [4]. However, the high cost, poor processing techniques, and high density of these metals can hinder their broad application in micro- or nano-scale electronic devices.

Graphene, in monolayer or few-layer forms, has been demonstrated to reach ultrahigh levels of thermal conductivity (up to ~5000 W/m·K) by both experiments and simulations [5–9]. Nevertheless, there are few reliable approaches to handle such atomically thin materials, which hampers their device-related applications [10]. Many researchers have worked to incorporate graphene into polymer matrices for nanocomposites with advanced functionality [11–16]. These nanocomposites achieve low density and high flexibility, as well as enhanced thermal conductivity, and are processing technologies that can be implemented fairly easily. Yet, limited by the undesirable thermal conductivity of polymer matrices (~0.1 W/m·K) and the high interfacial thermal resistance between graphene and polymer, the thermal conductivity of graphene nanocomposites (~1 W/m·K) is still much lower than

expected [17–21]. This low thermal conductivity of graphene nanocomposites makes it difficult to satisfy the requirement of efficient heat dissipation in micro/nano-electronic devices.

Recently, free-standing films obtained from graphene or graphene oxide (GO) have attracted loads of interest in the thermal management field due to their high thermal conductivity, superior electrical conductivity, and excellent mechanical properties [22–24]. Free-standing graphene films (GFs) could inherit the ultrahigh thermal conductivity of graphene, achieving a thermal conductivity above 3000 W/m·K [25]. Compared to the metals commonly used for heat dissipation, GFs possess a much lower density (<1 g/cm^3), superb flexibility as well as lower cost, demonstrating the potential for effective heat dissipation and use as thermal interfacial materials. In the past few years, numerous studies have been carried out to fabricate GFs with high thermal conductivity. However, it is noted that through different synthesis methods the GFs achieved substantially dissimilar thermal conductivity, varying from 30 to 3300 [25,26]. Thus, it is necessary to review recent advances in free-standing GFs to inform the design of GFs with advanced functionality.

In this review, we summarize the state of the art with regard to free-standing GFs in recent years. We focus on fabrication approaches as well as the thermal conductivity of the as-prepared GFs. The factors most influencing the thermal conductivity of GFs are identified and the impact of these factors is discussed. Several typical applications of the GFs for thermal management are also epitomized and discussed. The goal is to provide a concise overview of designing free-standing GFs with improved thermal conductivity.

2. Synthesis of Graphene-Based Films

There are several approaches to obtain graphene films with thickness in microns [27–29]. Similar to the fabrication of graphene, synthesis of graphene films follows two main procedures: "top-down" and "bottom-up". The top-down processes attain graphene films from graphite, including vacuum filtration [26,27,30–36], direct evaporation [37–39], and diverse coating techniques [28,40]. The bottom-up processes are based on the synthesis of graphene films from gaseous carbon sources, such as chemical vapor deposition [23].

2.1. Vacuum Filtration Method

Vacuum filtration is a convenient and widely-used top-down approach to assemble GFs. The pore size of filter films is controlled to make sure that the solvent molecules can permeate the filter paper easily, while graphene sheets remain on the surface of filter film. The typical process of the vacuum filtration strategy is illustrated in Figure 1. Graphite is adopted as the source material. Graphene oxide (GO) is first obtained from graphite powders via the well-established Hummers' method or modified Hummers' method [41]. Then GO solutions with various GO concentrations are prepared for the filtration. The thickness of the GO films can be tuned by modulating the GO concentration. The wet GO films can be fabricated after vacuum filtration for several minutes. Then, the GO film can be easily peeled off from the filter film after being dried at 80 °C for several minutes. In this stage, GO films show very low thermal conductivity due to the intrinsic low thermal conductivity of the GO. Thus, the GO films have to be reduced to GFs via high-temperature annealing. The annealing temperatures are as high as 3000 °C [28]. Such high temperatures can effectively graphitize the GO to graphene, leading to improved thermal conductivity of the final GFs. However, the use of such a high temperature for graphitization may hinder the wide application of GFs.

Not only the GO solution, but also the graphene solution can be directly applied in vacuum filtration for the GFs. For example, Teng et al. [34] applied a facile ball-milling approach to obtain large-volume, high-concentration, and plane-defect-free graphene dispersion in *N*-methyl-2-pyrrolidone (NMP) from graphite. After the filtration, annealing at 2850 °C for 2 h and a compression at 30 MPa, the obtained GFs exhibited superb electrical conductivity of 2.23 × 10^5 S/cm, and high thermal conductivity of 1529 W/m·K [34].

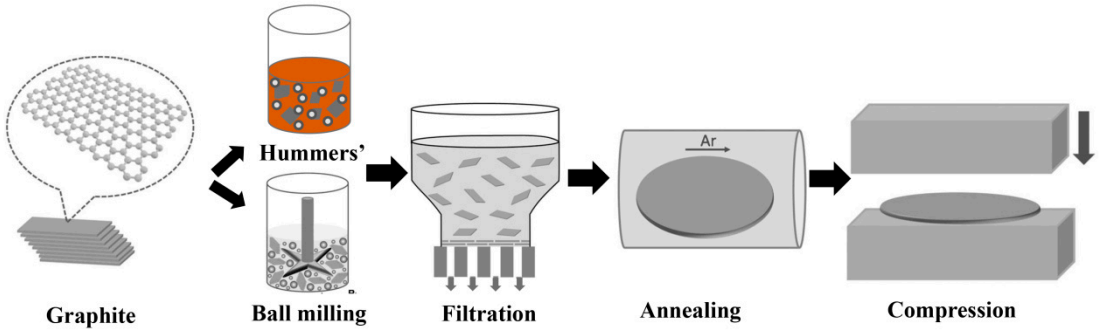

Figure 1. Schematic plot of the process of vacuum filtration for graphene films. Graphite can be oxidized to GO using Hummers' method, or exfoliated in ball milling. Reproduced and modified from [34] with permission; Copyright 2017 Wiley Online Library.

2.2. Direct Evaporation Method

The direct evaporation method is another simple approach to GF fabrication. In this method, the GO solution is poured into a container with a flat bottom, followed by continuous evaporation by heating the GO solution to a proper temperature. After several hours, the solvent (i.e., water) is evaporated and a thin film is left on the surface of the container. For instance, Shen et al. [37] used the direct evaporation method to attain the GFs. The GO solution was obtained by dissolving GO in water and the GO solution was poured into Teflon dishes for evaporation. Then, the Teflon dishes were heated to 50–60 °C for 6–10 h to evaporate the water and form GO films. The GO film was annealed at 2000 °C under argon flow for one hour after peeling off from the dishes. The dark, freestanding, and flexible GFs were obtained after the high-temperature annealing. The GFs have a superb in-plane thermal conductivity of about 1100 W/m·K. Similarly, Chen et al. applied the evaporation method to form GFs at the liquid/air interface [39]. The GO suspension was sonicated to exfoliate GO sheets and centrifuged to remove impurities. The obtained GO hydrosol was heated to 80 °C for different times to get films of different thicknesses. The condensed thin film formed very rapidly at the liquid/air interface. After drying at 80 °C for 8 h, smooth and free-standing GFs were obtained.

The GO solution or graphene solution with high concentration can be directly coated onto a substrate for the evaporation step, rather than poured in containers. Recently, Peng et al. [28] scraped a GO suspension (10–20 mg·mL^{-1}) with a thickness of 0.5–5 mm on copper foil and kept evaporating the water at room temperature for 24 h. The as-prepared GO film was carbonized at 1300 °C for 2 h and graphitized at a high temperature of 3000 °C for 1 h under argon flow. After cooling slowly to room temperature, the GF was compressed under a pressure of 50 MPa for 15 min, 100 MPa for 30 min, and 300 MPa for 1 h to form a dense GF. In this method, GFs with a large surface area can be easily obtained by utilizing copper foil. The copper foil can also be recycled for low-cost, large-scale fabrication of GFs [42].

It is noted that in vacuum filtration and direct evaporation, thermal annealing is not the only way to reduce a GO film to graphene films. Chemical reduction is also a broadly-used approach to reduce GO to rGO. The reducing agents can be either organic or inorganic chemicals, such as ascorbic acid and HI acid [43–46]. Yang et al. applied HI acid to reduce the GO/cellulose composite film from vacuum filtration [47]. The obtained composite film exhibited an in-plane thermal conductivity of 7.3 W/m·K, and a strong anisotropy in thermal conductivity. Jin et al. compared the effect of different reduction methods on the thermal conductivity of the GFs [48]. They used HI acid, thermal reduction at 600 °C and the combination of HI acid and thermal conduction to reduce the GO films to the GFs. It is demonstrated that thermal reduction is the best way to achieve GFs with higher thermal conductivity, compared with other reduction methods.

2.3. Other Assembling Methods

Besides the aforementioned vacuum filtration and direct evaporation methods, there are also some other top-down methods to fabricate GFs, such as spray coating [24,49,50], spin casting [51,52], and roll-to-roll manufacturing [53]. For instance, Xin et al. [40] adopted a novel approach integrating electron-spray deposition (ESD) and a roll-to-roll device to manufacture the free-standing GFs with large area; the process is illustrated in Figure 2. In the ESD process (Figure 2a), tiny droplets were generated by the repulsion force between electrical charges and the droplets, while the size of the droplets could be controlled by adjusting the flow speed and electric field. The electric field between nozzle and substrate allowed the droplets to distribute uniformly on the surface of the substrate. Simultaneously, the heating plate could evaporate the solvent, leaving the GFs on the surface of the substrate. A roll-to-roll device was employed to obtain GFs with a large area, shown in Figure 2b. This combined facility opens up the possibility of manufacturing GFs on a large scale, which may be adopted in the industrial manufacturing of GFs.

In summary, for the top-down strategies for GFs, we can conclude that all of them obtain GFs from GO or graphene nanosheets via different assembling techniques. To achieve high thermal conductivity of the GFs, high-temperature thermal annealing or chemical reduction is often conducted.

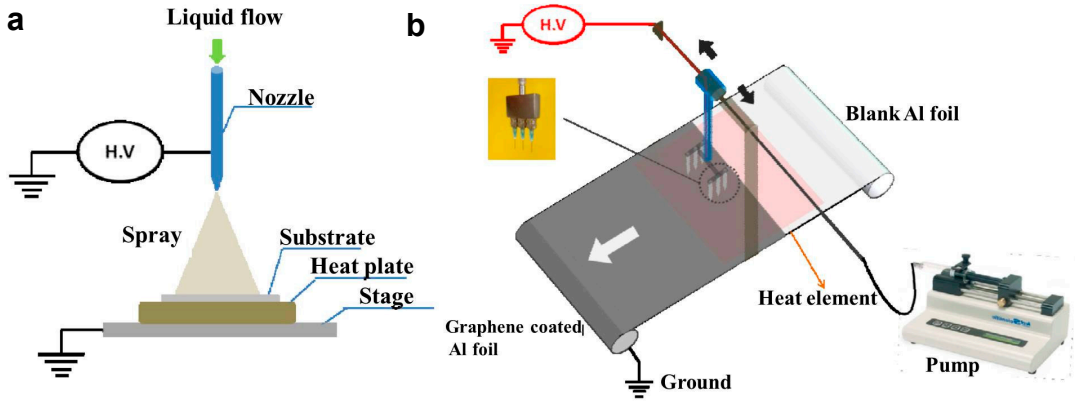

Figure 2. Schematic plot of (**a**) electron-spray deposition and (**b**) roll-to-roll device with a pump. Reproduced from [40] with permission; Copyright 2014 Wiley Online Library.

2.4. Chemical Vapor Deposition

Chemical vapor deposition (CVD) is the typical bottom-up strategy to fabricate a high-quality graphene film with controllable thickness. Ma et al. developed a segregation-adsorption CVD (SACVD) to grow a well-stitched high-quality monolayer graphene film with a tunable uniform grain size from 200 nm to 1 μm on a Pt substrate [23]. They found that the thermal and electrical conductivity of the GF could be tuned by modulating the grain size of graphene. The high-quality graphene film from SACVD with tunable thermal and electrical conductivity can be directly used in electronic, optoelectronic, and thermoelectric applications. However, the transfer of GFs from the Pt substrates may be difficult, limiting their broad application. Thus, the non-substrate CVD approach is preferred to effectively fabricate GFs [54]. Hu et al. combined CVD and spray coating to synthesize CNT/graphene composite films [54]. Spinnable CNT arrays were continuously synthesized and collected by a rotating mandrel from a CVD furnace. During the collection of CNT arrays, the GO aqueous solution was sprayed onto the winding mandrel, as illustrated in Figure 3. After thermal annealing at 2800 °C, the composite films achieved a high thermal conductivity of 1056 W/m·K and a superior mechanical strength of ~1 GPa. A combination of CVD and other simple techniques can be used for the large-scale fabrication of high-quality GFs.

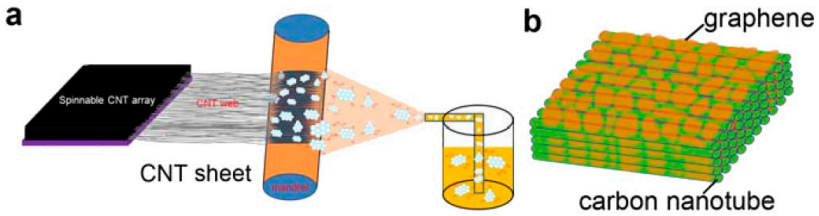

Figure 3. Schematic plot of CVD and the spray-coating process (**a**), and the obtained free-standing CNT array/GO composite films (**b**). Reprinted from [54] with permission; Copyright 2017 Elsevier.

3. Thermal Transport Properties of Free-Standing Graphene Films

3.1. Macro- and Micro-Scale Morphologies of Free-Standing Graphene Films

The GFs fabricated by different methods normally exhibited different macro-scale morphology, but similar micro-scale morphology due to the involved high-temperature annealing. As shown in Figure 4a, after vacuum filtration the GO films displayed a dark brown color and had a rounded shape due to the filtration membranes used in the process [36]. After reduction using HI acid, the rGO films had a shiny metallic color (Figure 4b) and excellent flexibility (Figure 4c). Scanning electron microscope (SEM) images showed that the thickness of the GO films after vacuum filtration was around 10 μm (Figure 4d) and the thickness decreased to ~7.5 μm after the HI reduction (Figure 4e). The layered structures can be clearly observed in the SEM cross section images. Different from the GFs obtained via the chemical reduction, the GFs experiencing high-temperature annealing were normally gray and had wrinkles on the surface [48]. The thermal annealing also caused air pores in the GFs (Figure 5), decreasing the thermal conductivity of the GFs. Therefore, high-pressure compression is always conducted to remove air pores from the GFs. Compared to the GFs obtained by the vacuum filtration method, the GFs from other top-down strategies can have a larger area and a different shape [22]. All these GFs obtained from the top-down strategies show excellent flexibility, as seen in Figure 6, where the GFs can be folded into complex structures [22].

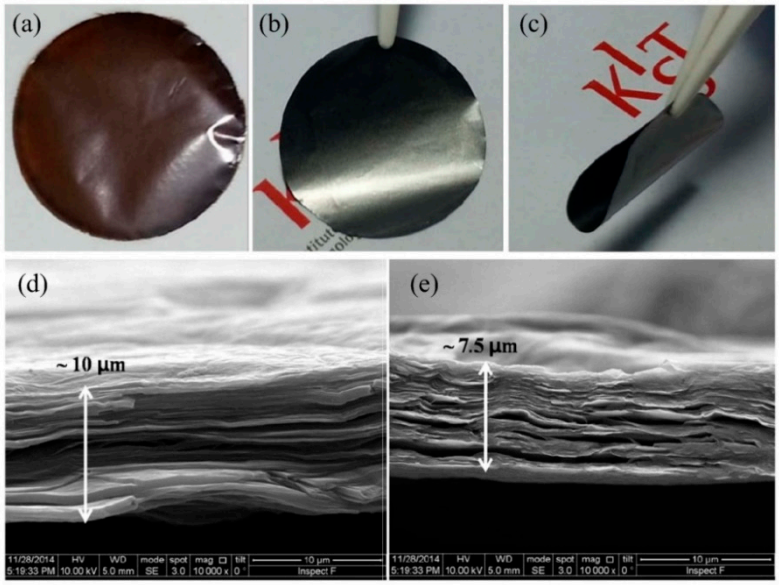

Figure 4. Macro-scale morphology of (**a**) the free-standing dark-brown GO film; (**b**,**c**) are HI reduced shiny metallic and flexible rGO films; (**d**,**e**) are cross-sectional SEM images of as-prepared GO and rGO films, respectively. Reprinted from [36] with permission; Copyright 2015 Elsevier.

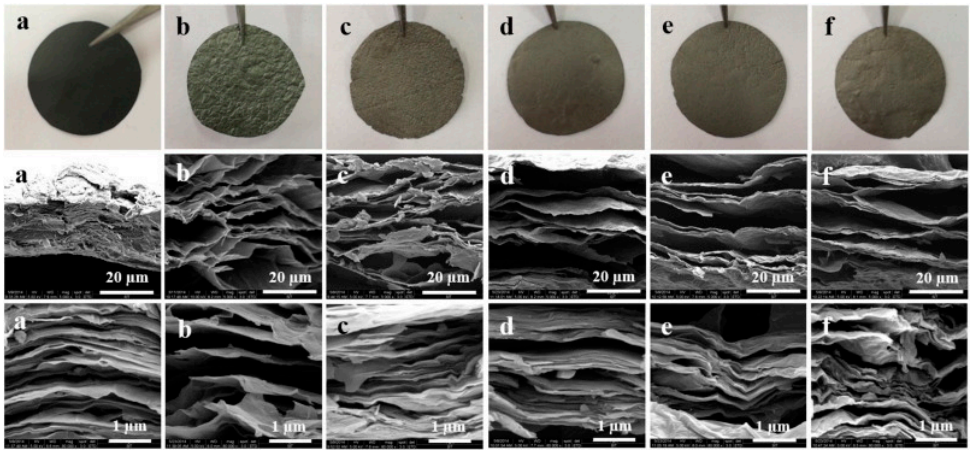

Figure 5. Visual (top), low-magnification SEM (middle), and high-magnification SEM (bottom) images of (**a**) GO film; (**b**) rGO film with HI recution; (**c**) rGO film with HI reduction + 600 °C reduction; (**d**) rGO film with 600 °C reduction; (**e**) rGO film with 800 °C reduction; and (**f**) rGO film with 1000 °C reduction. Reprinted from [48] with permission; Copyright 2015 Elsevier.

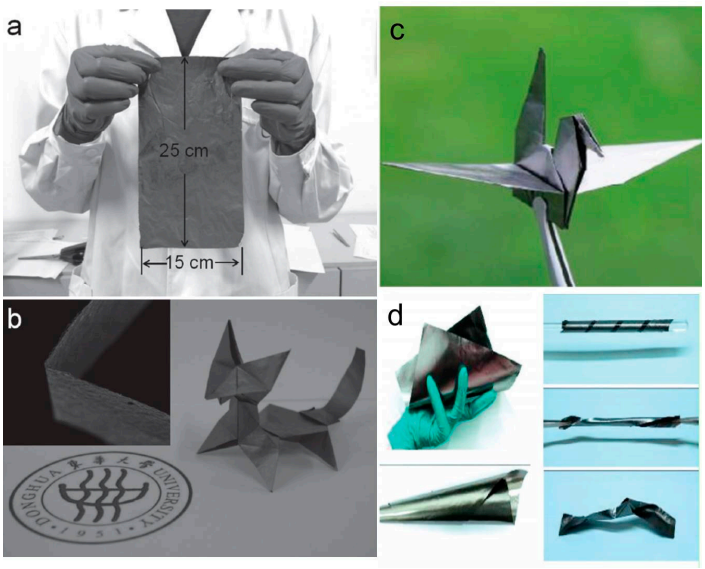

Figure 6. (**a**) Large-area and free-standing GF from direct evaporation; (**b**) sharply folded and twisted craft from the GF; (**c**) a piece of GF was folded into a crane without breakages; and (**d**) the GF in the states of bending, curling, enwinding, twisting and knotting. (**a**,**b**) Reprinted from [22] with permission, Copyright 2017 Wiley Online Library; (**c**,**d**) Reprinted from [28] with permission, Copyright 2017 Wiley Online Library.

3.2. Thermal Conductivity of Free-Stranding Graphene Films

Graphene has been demonstrated to have ultrahigh thermal conductivity [46,55,56]. Baladin et al. measured the thermal conductivity of a graphene monolayer and found that it exceeded 3000 W/m·K near room temperature via optothermal Raman measurement [57,58]. A recent study revealed that phonons had a mean free path of ~28 μm in CVD-grown graphene, which makes phonons rather than electrons dominate the thermal conduction in graphene, leading to $K_e << K_p$ [59]. As GFs are composed of graphene, they are expected to inherit the high thermal conductivity of graphene. However, it is found that GFs exhibited thermal conductivity in a large range of 30–3300 W/m·K [25,26], which may be because of the following reasons:

1. Different fabrication methods: different fabrication methods produced GFs with different crystal structures. Top-down strategies of fabricating GFs from GO always induced lower thermal conductivity compared to those obtained from bottom-up strategies, which may produce different and clean crystal structures of the GFs.
2. Different reduction methods: in top-down strategies, different reduction methods, such as thermal annealing and chemical reduction, also result in different thermal conductivity of the GFs. Different temperatures in thermal reduction and different reducing agents in chemical reduction lead to different thermal conductivity.
3. Different post-treatment methods: GFs with or without compression or compressed under different pressure exhibited dissimilar thermal conductivity.

Yu and colleagues [26] modified GO with alkaline earth metal ions to fabricate GO films with tuned thermal conductivity. The GO films modified with Mg^{2+} and Ca^{2+} acquired enhanced thermal conductivity of 32.05 W/m·K and 61.38 W/m·K, respectively, which are more than 8 and 15 times that of crude GO films (3.91 W/m·K). Gee et al. prepared the GFs through an electrochemical exfoliation and filtration process [25]. The thermal conductivity of the as-prepared GFs was measured to be 3390 W/m·K by using the thermoelectric method. This is the highest reported thermal conductivity of GFs, which is even much higher than that of graphite (K_i = 2000 W/m·K) [58,60].

Peng et al. obtained the GO films through a scrape coating and direct evaporation [28]. After carbonized at 1300 °C and graphitized at 3000 °C, as well as compressed at 50–300 MPa, the rGO films exhibited a thermal conductivity as high as 1940 ± 113 W/m·K. This may be because (i) the high temperature (3000 °C) can reduce the functional groups on graphene (transforming the sp^3 crystal of GO to the sp^2 crystal of graphene), and (ii) the high temperature can also promote the self-healing of the defective graphene, inducing perfect graphene with sp^2 crystals. Both the functional group-free and defect-free crystals benefit from the thermal conduction in the GFs. Guo et al. combined blade-coating and direct evaporation to fabricate self-standing GO films [22]. After being reduced by vitamin C, the rGO films achieved a high thermal conductivity of 2600 W/m·K. For comparison, the thermal conductivity of the GFs synthesized using different methods is summarized in Table 1.

Table 1. Summary of the GFs obtained from different synthesis method.

Materials	Fabrication Method	Reduction Method/Post-Treatment	Thermal Measurement	Thermal Conductivity (W/m·K)
Graphene film [25]	Electrochemical exfoliation, vacuum filtration	–	Thermoelectric method	3300
rGO film [22]	Blade-coating, evaporation	Vitamin C reduction	Laser flash	2600
rGO film [28]	Scrape coating, evaporation	Annealed at 3000 °C, compressed at 50–300 MPa	Laser flash	1940
Graphene film [61]	Hydroxide-assisted exfoliation, vacuum filtration	Annealed at 2800 °C, compressed at 100 MPa	Laser flash	1842
rGO film [33]	Vacuum filtration	L-ascorbic acid reduction	Laser flash	1642
Graphene film [34]	Ball-milling, Filtration	Annealed at 2850 °C, compressed at 30 MPa	Self-heating	1529
rGO film [36]	Vacuum filtration	HI reduction	Laser flash	1390 ± 65
rGO film [62]	Vacuum filtration	Annealed at 1200 °C	Laser flash	1043.5
rGO film [42]	Evaporation	Annealed at 900 °C in 5% H_2-Ar gas	Laser flash	902
rGO film [63]	Roller coating	Annealed at 2800 °C	Laser flash	826
rGO film [48]	Filtration	Annealed at 1000 °C	Laser flash	373
Graphene nanoplatelet film [35]	Vacuum filtration	Annealed at 120 °C and 340 °C	Laser flash	313
rGO film [31]	Vacuum filtration	Annealed at 1060 °C	Angstrom method	220
rGO film [26]	Vacuum filtration	Metal ion modified	Laser flash	Mg-modified: 32.05 Ca-modified: 61.38
rGO film [38]	Direct evaporation	Annealed at 1000 °C	Laser flash	61

3.3. Parameters That Affect the Thermal Conductivity of Free-Standing Graphene Films

3.3.1. Thermal Annealing Temperature

GO has various functional groups and defects in its surface. Thermal annealing in a proper temperature may partially reduce GO to rGO, thus leading to the higher thermal conductivity of the GFs. Previous studies have corroborated that the thermal annealing temperature exerts a significant impact on the thermal conductivity of the GFs [28,37,38,40]. Renteria et al. [38] studied the effect of thermal annealing temperature on the thermal conductivity of the rGO films. The in-plane thermal conductivity of the rGO films dramatically increased from ~3 to ~61 W/m·K (room temperature) when GO films were annealed up to 1000 °C, as presented in Figure 7a. More recently, Peng et al. also found that the thermal conductivity of rGO films could be elevated by raising the annealing temperature [28]. The thermal conductivity of the rGO films increased from ~800 to ~2000 W/m·K (close to that of graphite) as the annealing temperature was raised from 1400 °C to 3000 °C, as displayed in Figure 7c.

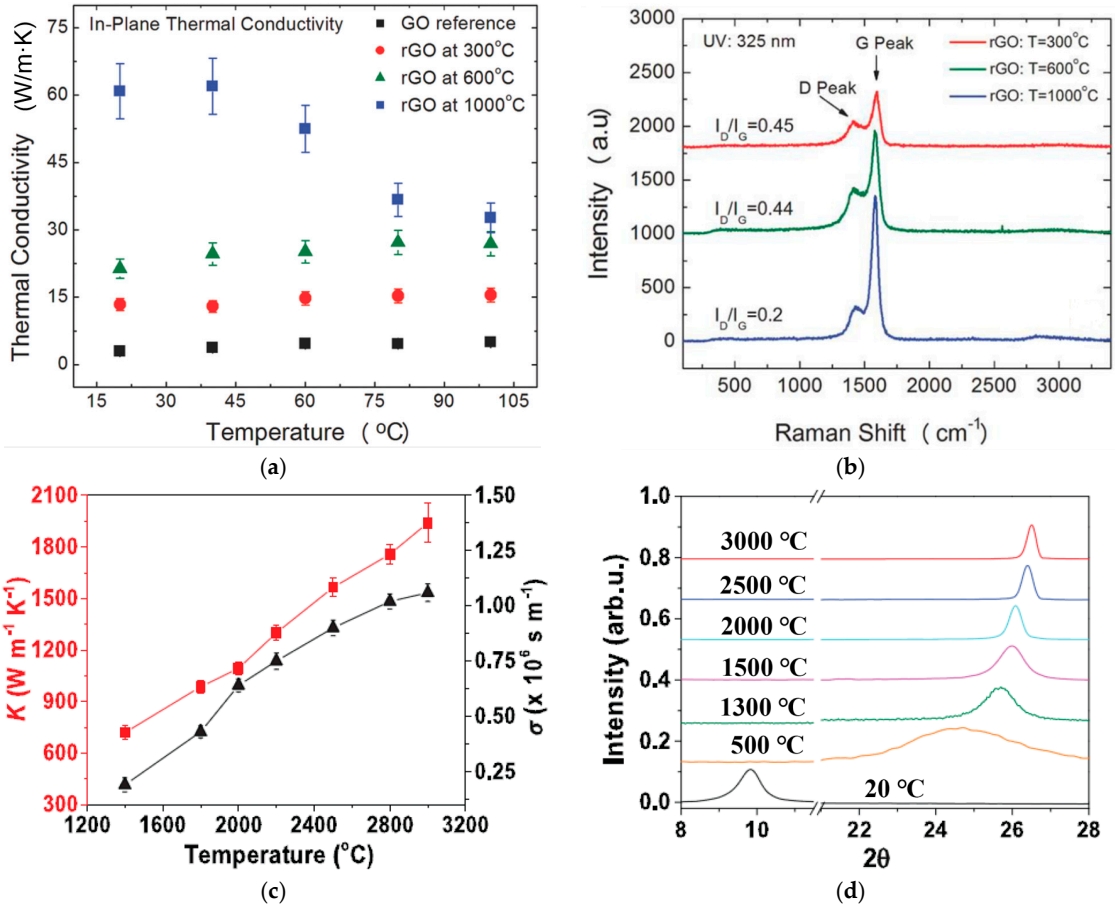

Figure 7. (**a**) Experimental in-plane thermal conductivity, *K*, as a function of temperature for rGO films annealed at different temperatures and a reference GO film. (**b**) Raman spectra of rGO films under UV (λ = 325 nm) laser excitations. The peaks at ≈1350 and 1580 cm^{-1} correspond to the D and G peaks, respectively. (**c**) The thermal (red line) and electrical conductivity (black line) of rGO films annealed at different temperatures. (**d**) XRD patterns of rGO films annealed at different temperatures. (**a**,**b**) Reprinted from [38] with permission, Copyright 2015 Wiley Online Library; (**c**,**d**) Reprinted from [28] with permission, Copyright 2017 Wiley Online Library.

The thermal conductivity increase with the rise of annealing temperature may be caused by the removal of the functional groups and defects of GO films, as well as the recovery of the sp^2 crystal structures from the sp^3 crystal. This was substantiated by the decreased I_D/I_G ratio in Raman

spectroscopy and the different peaks in X-ray powder diffraction (XRD) patterns with raising the annealing temperature (Figure 7b,d). In addition to the thermal annealing temperature, the gas atmosphere during thermal annealing also affects the final thermal conductivity of the rGO films. Introducing a reducing gas, like H_2, could lead to a higher thermal conductivity of the rGO films. For instance, Liu et al. thermally annealed GO films at 900 °C in a 5% H_2-Ar gas mixture and the as-prepared rGO films obtained have a thermal conductivity as high as ~1200 W/m·K [64]—much higher than those annealed without H_2 at the same temperature [38].

3.3.2. The Lateral Size of Graphene and GO Sheets

Compared to electrons, phonons dominate the thermal conduction in graphene and related nanomaterials. Phonons exhibited a mean free path (MFP) as long as 28 μm in CVD-grown graphene, and the heat was found to be transferred through a ballistic mechanism in graphene and rGO [58,65]. The size of graphene or rGO has been demonstrated to greatly affect the thermal conductivity of the GFs in both experimental and theoretical studies [66–68], especially when the graphene size is close to or smaller than the MFP. Ma et al. tailored the thermal transport properties of graphene films by modulating the grain size of graphene [23]. They applied a segregation-adsorption CVD to grow graphene films with a tunable grain size from ~0.2 μm to ~10 μm. With increasing the grain size of graphene, the obtained GFs displayed a dramatic increase in thermal conductivity (0.5~5.2 × 10^3 W/m·K). Peng et al. [28] also reported the obvious elevation from ~1000 W/m·K to ~1950 W/m·K for the thermal conductivity of the as-prepared debris-free graphene films (dfGFs) when the average size of the graphene sheets increased from ~5 μm to 100 μm.

Kumar et al. [36] fabricated small rGO films (rSGO) and a large-area rGO film (rLGO) and compared their thermal and electrical conductivity. The rSGO films exhibited a thermal conductivity of 900 W/m·K, while the rLGO films exhibited a thermal conductivity of 1390 W/m·K, indicating that higher thermal conductivity of rGO films can be achieved by utilizing large GO sheets. Reducing the size of graphene sheets not only shortens the mean free path of phonons in graphene sheets, but also increases the phonon scattering probability in the films, thus inducing lower thermal conductivity of the graphene films. The thermal conductivity of the graphene films may be turned by using the graphene or graphene oxide with a different size [36,69].

3.3.3. Hybridization with Other Components

To enhance the thermal conductivity of GFs, graphene or GO can be combined with other materials to form hybrids. Kong et al. randomly deposited carbon fiber (CF) as the porous scaffold on the porous metal plates through vacuum filtration [27]. Then GO hydrogel was subsequently deposited on the porous scaffold to form GO–CF composite (G–CF) films. After annealing at 1000 °C in Ar atmosphere, the as-prepared G-CF films exhibited a superior thermal conductivity of 977 W/m·K, significantly higher than those of graphene film (318 W/m·K), graphitized polymide (PI) film (743 W/m·K), and flexible graphite film (137 W/m·K). Hu et al. also combined a carbon nanotube (CNT) film with GO for hybrid films by applying CVD and a spray-coating method [54]. The as-prepared GO/CNT composite films were thermally annealed at 2800 °C to reduce GO to rGO. The rGO/CNT films delivered a high thermal conductivity of 1056 W/m·K, a superior mechanical strength of ~1 GPa, and an excellent electrical conductivity of 1182 S/cm.

Besides CNTs and CFs, other diverse materials have also been used in combination with graphene for advanced functional properties, such as polymers [70–72] and various 2D materials [73–75]. The graphene/polymer composite films generally attain a lower thermal conductivity compared to the pure graphene films. This may be due to the ultralow thermal conductivity of the polymer (~0.1 W/m·K) compared to that of graphene (>100 W/m·K), transforming the ballistic heat transfer in graphene to the diffusive heat transfer in polymers [76,77]. Moreover, a number of theoretical studies have demonstrated that the interfacial thermal resistance (often known as the Kapitza resistance) between graphene and polymer also lowers the thermal conductivity of the composite films [78–81].

The interfacial thermal resistance arises from poor thermal coupling between graphene and polymer, and can be significantly decreased by grafting the graphene sheets with polymer chains. However, excessive loading of grafted polymer may reduce the thermal conductivity of the graphene sheets, thus inducing lower effective thermal conductivity for the composite film. Therefore, the grafting density should be well-controlled to achieve a higher thermal conductivity of the composite film than the conductivity of the polymer matrix [81]. More discussion about nanoscale thermal transport based on phonon propagation can be found in other reviews [82,83]. When combining graphene and other nanomaterials with high thermal conductivity, like boron nitride (BN) or CNTs, the composite films still can achieve a desirable thermal conductivity. This may be due to low interfacial thermal resistances between graphene and other nanomaterials, owing to the strong phonon—phonon coupling [84,85]. Table 2 is a presentation of the typical hybrid films reported in the past three years, clearly manifesting the effects of different hybridization components on the thermal conductivity of the hybrid films.

Table 2. Summary of the graphene composite films combined with different materials.

Materials	Fabrication Method	Reduction Method/Post-Treatment	Thermal Measurement	Thermal Conductivity (W/m·K)
rGO/CNT film [54]	CVD, spray coating	Annealed at 2800 °C	Laser flash	1056
rGO/carbon fiber film [27]	Vacuum filtration	Annealed at 1000 °C	Laser flash	977
rGO/PBO film [86]	Dispersion, casting	120 °C to reduce GO	Laser flash	50
BN/GO film [87]	Vacuum filtration	–	Laser flash	29.8
GO/polymer/BN film [88]	casting	–	Laser flash	12.62
rGO/cellulose film [89]	Vacuum filtration	Hydrazine reduction	Laser flash	6.17
Graphene/PI film [90]	CVD/impregnation	–	Laser flash	3.73
Graphene/NRlatex film [91]	Ball milling dipping	–	Hot-disk	0.482
GO/MWNT films [92]	Vacuum filtration	–	Laser flash	0.35

3.3.4. Thickness and Density of the Graphene Films

The thickness of graphene films also plays a significant role in the thermal conductivity of graphene films. Zhang et al. compared the thermal conductivity of the GFs with different thicknesses from 20 to 60 μm [33]. They found that the in-plane thermal conductivity of the GFs decreased from 1642 W/m·K to 675 W/m·K as the thickness increased from 20 μm to 60 μm. This phenomenon was due to the enhancement of total defects in graphene films with bigger thickness. More defects would result in a more significant scattering of phonons, thus hindering the phonon propagation along the in-plane direction.

Not only the thickness, but also the density of the GFs would influence the thermal conductivity of the GFs. Xin et al. [40] conducted compaction to remove air pores to fabricate dense GFs, but with different density. Even at different annealed temperatures, the thermal conductivity of the GFs significantly elevated with the increase in the GFs' density. As shown in Figure 8, for the 2850 °C annealed GFs, when the density increased from 0.4 g/cm^3 to 2.0 g/cm^3, the thermal conductivity of the GFs increased from 200 W/m·K to ~1500 W/m·K. The significant increase of thermal conductivity of the GFs with the rise of density may be explained as described below:

i. Higher density means fewer air pores in the GFs, which may reduce the phonon scattering at air–graphene interfaces, thus inducing the higher thermal conductivity of the GFs.
ii. According to the equation ($K = \alpha\rho C_p$) used to calculate the thermal conductivity of the GFs, given thermal diffusivity α and specific capacity C_p, the thermal conductivity, K, increases linearly with density, ρ. As shown in Figure 8, the values of K show an approximately linear relationship with ρ.

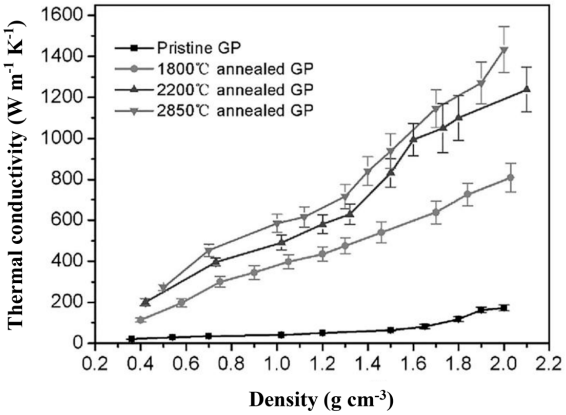

Figure 8. Change of thermal conductivity of free-standing graphene films with different density under different annealed temperatures. Reprinted with permission from [40]; Copyright 2014 Wiley Online Library.

4. Applications of Free-Standing Graphene Films in Thermal Engineering

The outstanding thermal conductivity of the GFs contributes to promising applications in diverse thermal management fields, such as thermal interface materials (TIMs), and heat dissipation materials (HDMs). For instance, to demonstrate the thermal management capabilities of their rGO films, Huang et al. applied a 7 W high-bright LED as a hot spot and recorded the temperature changes by a thermocouple sensor in the systems with and without rGO films [63], as illustrated in Figure 9a. The rGO films effectively reduced the temperature of the LED hot spot, 3 °C difference after few minutes shown in Figure 9b, confirming the heat dissipation ability of the as-prepared rGO films.

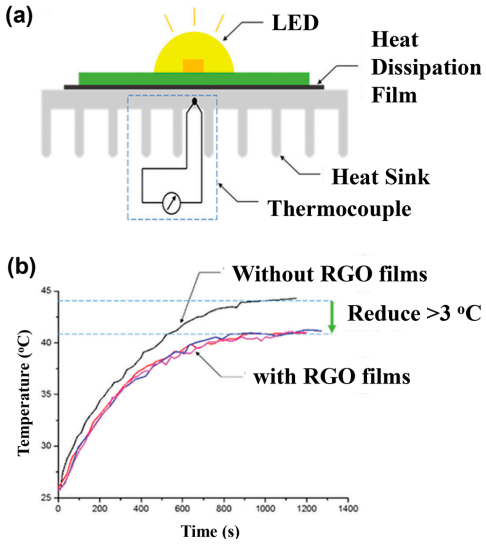

Figure 9. (**a**) Schematic plot of the temperature measurement model of a 7 W LED as the hot spot with and without rGO films. (**b**) Real-time temperature profile of the LED hot spot with and without rGO films. Reprinted from [63] with permission; Copyright 2017 Royal Society of Chemistry.

Guo et al. fabricated ultra-flexible, lightweight, and stretchable rGO films for wearable thermal management components [22]. They designed the rGO films into kirigami structures and integrated them into cloth for personal thermal management, as displayed in Figure 10. With a small applied voltage (3.2 V), a rapid heating-up response to 45 °C from room temperature could be achieved in 6 s. When the heating stopped, the rGO films cooled down to room temperature in 5 s, manifesting both fast

electrical heating response and efficient heat dissipating capability. Zhang et al. also demonstrated the superb performance of the GFs as TIMs in microelectronic devices [33]. When combined with functional GO (FGO), the GFs exhibited a better TIMs performance due to the reduced thermal resistance between the GFs and the microelectronic chips by the FGO. Besides thermal management applications, GFs and related films can also be applied in various other applications, such as electromagnetic interference (EMI) shielding, gas barriers, and energy storage and sensors [35,36,88,93–100], owing to their superior electrochemical and mechanical properties.

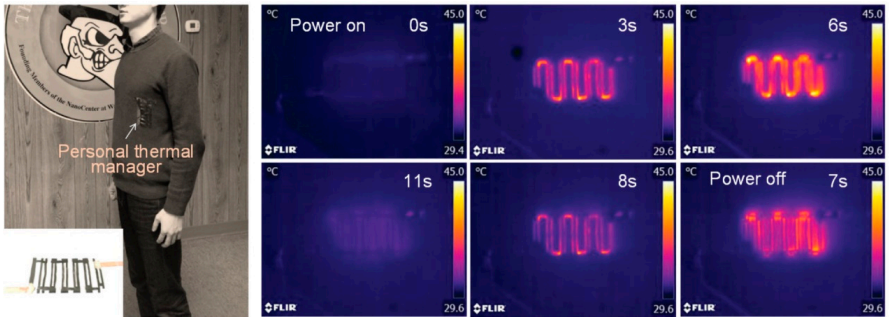

Figure 10. A demonstration of wearable rGO films for personal thermal management. The rGO films possessed kirigami structure and were integrated into cloth. A work cycle of heating–cooling can be implemented within 11 s. Reprinted from [22] with permission; Copyright 2017 Wiley Online Library.

5. Summary and Outlook

In this article, we have reviewed recent advances in the subject of thermal conductivity of free-standing GFs. Diverse "top-down" strategies, like vacuum filtration, direct evaporation, and various coating techniques, have been developed to prepare free-standing GFs with large areas. "Bottom-up" CVD methods can be used to synthesize GFs with high-quality crystals. For GFs obtained from the GO, thermal annealing is normally required to reduce the GO and even to graphitize the rGO films for high thermal conductivity. Higher annealing temperature generally results in heightened thermal conductivity of the GFs. The thermal conductivity of the GFs can be also enhanced by hybridizing with other conducting materials, decreasing the GF thickness, increasing the GFs density, as well as completely reducing the GO. The high thermal conductivity of the GFs enables them to be utilized in extensive thermal management applications, such as highly efficient heat-dissipating materials and thermal interfacial materials.

In existing studies, thermal annealing at high temperature, as high as 3000 °C, was carried out to reduce the GO and, thus, to heighten the thermal conductivity of the GFs. However, thermal annealing at such a high temperature is not practical, and is also an energy-consuming process, which may hinder the industrial manufacturing of GFs with this method. Therefore, new reduction approaches that are low-cost, environmentally friendly, and easily accessible should be the new research direction. In addition, a lot of previous investigations pursued the high thermal conductivity of the GFs rather than considering the realistic applications of GFs. For instance, few studies took into account the contact between the GFs and the hot spot substrates: ineffective contact between the GFs and substrates may induce high thermal contact resistance, thus significantly lowering the efficiency of the GFs. More effort should be made to integrate the GFs into the micro-/nano-electronic devices with compact size and low weight for broader applications of the GFs. Multi-scale theoretical modeling, like molecular dynamics simulations and finite element methods, can be involved to shed light on the heat transfer mechanisms in the GFs from the atomic scale to the macro-scale. More attention should also be paid to combining different techniques, either "top-down" or "bottom-up," to achieve the large-scale fabrication of the GFs for industrial applications, for example, acting as packaging materials in high-power battery packs for whole electrical vehicles.

Acknowledgments: We appreciate the financial support from the National Natural Science Foundation of China (51602038), the Sichuan Science and Technology Agency (2017HH0101, 2017GZ0113), and the Fundamental Research Funds for the Central Universities (ZYGX2016KYQD148).

Conflicts of Interest: The authors declare no conflicts of interest.

References

1. Zhu, H.; Li, Y.; Fang, Z.; Xu, J.; Cao, F.; Wan, J.; Preston, C.; Yang, B.; Hu, L. Highly thermally conductive papers with percolative layered boron nitride nanosheets. *ACS Nano* **2014**, *8*, 3606–3613. [CrossRef] [PubMed]
2. Chen, H.; Ginzburg, V.V.; Yang, J.; Yang, Y.; Liu, W.; Huang, Y.; Du, L.; Chen, B. Thermal conductivity of polymer-based composites: Fundamentals and applications. *Prog. Polym. Sci.* **2016**, *59*, 41–85. [CrossRef]
3. Moore, A.L.; Shi, L. Emerging challenges and materials for thermal management of electronics. *Mater. Today* **2014**, *17*, 163–174. [CrossRef]
4. Thermal Conductivity of common Materials and Gases. Available online: https://www.engineeringtoolbox.com/thermal-conductivity-d_429.html (accessed on 7 February 2018).
5. Hu, J.; Ruan, X.; Chen, Y.P. Thermal conductivity and thermal rectification in graphene nanoribbons: A molecular dynamics study. *Nano Lett.* **2009**, *9*, 2730–2735. [CrossRef] [PubMed]
6. Yan, Z.; Nika, D.L.; Balandin, A.A. Thermal properties of graphene and few-layer graphene: Applications in electronics. *IET Circuits Devices Syst.* **2015**, *9*, 4–12. [CrossRef]
7. Shahil, K.M.F.; Balandin, A.A. Graphene-multilayer graphene nanocomposites as highly efficient thermal interface materials. *Nano Lett.* **2012**, *12*, 861–867. [CrossRef] [PubMed]
8. Zhang, H.; Fonseca, A.F.; Cho, K. Tailoring thermal transport property of graphene through oxygen functionalization. *J. Phys. Chem. C* **2014**, *118*, 1436–1442. [CrossRef]
9. Shahil, K.M.F.; Balandin, A.A. Thermal properties of graphene and multilayer graphene: Applications in thermal interface materials. *Solid State Commun.* **2012**, *152*, 1331–1340. [CrossRef]
10. Gong, F.; Liu, X.; Yang, Y.; Xia, D.; Wang, W.; Duong, H.; Papavassiliou, D.; Xu, Z.; Liao, J.; Wu, M. A facile approach to tune the electrical and thermal properties of graphene aerogels by including bulk MoS_2. *Nanomaterials* **2017**, *7*, 420. [CrossRef] [PubMed]
11. Fan, Z.; Gong, F.; Nguyen, S.T.; Duong, H.M. Advanced multifunctional graphene aerogel–poly (methyl methacrylate) composites: Experiments and modeling. *Carbon* **2015**, *81*, 396–404. [CrossRef]
12. Fang, X.; Fan, L.-W.; Ding, Q.; Wang, X.; Yao, X.-L.; Hou, J.-F.; Yu, Z.-T.; Cheng, G.-H.; Hu, Y.-C.; Cen, K.-F. Increased thermal conductivity of eicosane-based composite phase change materials in the presence of graphene nanoplatelets. *Energy Fuels* **2013**, *27*, 4041–4047. [CrossRef]
13. Dai, W.; Yu, J.; Liu, Z.; Wang, Y.; Song, Y.; Lyu, J.; Bai, H.; Nishimura, K.; Jiang, N. Enhanced thermal conductivity and retained electrical insulation for polyimide composites with sic nanowires grown on graphene hybrid fillers. *Compos. Part A Appl. Sci. Manuf.* **2015**, *76*, 73–81. [CrossRef]
14. Qian, R.; Yu, J.; Wu, C.; Zhai, X.; Jiang, P. Alumina-coated graphene sheet hybrids for electrically insulating polymer composites with high thermal conductivity. *RSC Adv.* **2013**, *3*, 17373–17379. [CrossRef]
15. Yu, L.; Park, J.S.; Lim, Y.S.; Lee, C.S.; Shin, K.; Moon, H.J.; Yang, C.M.; Lee, Y.S.; Han, J.H. Carbon hybrid fillers composed of carbon nanotubes directly grown on graphene nanoplatelets for effective thermal conductivity in epoxy composites. *Nanotechnology* **2013**, *24*, 155604. [CrossRef] [PubMed]
16. Luan, V.H.; Tien, H.N.; Cuong, T.V.; Kong, B.-S.; Chung, J.S.; Kim, E.J.; Hur, S.H. Novel conductive epoxy composites composed of 2-D chemically reduced graphene and 1-D silver nanowire hybrid fillers. *J. Mater Chem.* **2012**, *22*, 8649–8653. [CrossRef]
17. Wang, F.; Drzal, L.T.; Qin, Y.; Huang, Z. Enhancement of fracture toughness, mechanical and thermal properties of rubber/epoxy composites by incorporation of graphene nanoplatelets. *Compos. Part A Appl. Sci. Manuf.* **2016**, *87*, 10–22. [CrossRef]
18. Han, Z.D.; Fina, A. Thermal conductivity of carbon nanotubes and their polymer nanocomposites: A review. *Prog. Polym. Sci.* **2011**, *36*, 914–944. [CrossRef]
19. Gong, F.; Duong, H.; Papavassiliou, D. Review of recent developments on using an off-lattice monte carlo approach to predict the effective thermal conductivity of composite systems with complex structures. *Nanomaterials* **2016**, *6*, 142. [CrossRef] [PubMed]

20. Bui, K.; Duong, H.M.; Striolo, A.; Papavassiliou, D.V. Effective heat transfer properties of graphene sheet nanocomposites and comparison to carbon nanotube nanocomposites. *J. Phys. Chem. C* **2011**, *115*, 3872–3880. [CrossRef]
21. Konatham, D.; Bui, K.N.D.; Papavassiliou, D.V.; Striolo, A. Simulation insights into thermally conductive graphene-based nanocomposites. *Mol. Phys.* **2011**, *109*, 97–111. [CrossRef]
22. Guo, Y.; Dun, C.; Xu, J.; Mu, J.; Li, P.; Gu, L.; Hou, C.; Hewitt, C.A.; Zhang, Q.; Li, Y.; et al. Ultrathin, washable, and large-area graphene papers for personal thermal management. *Small* **2017**, *13*, 1702645. [CrossRef] [PubMed]
23. Ma, T.; Liu, Z.; Wen, J.; Gao, Y.; Ren, X.; Chen, H.; Jin, C.; Ma, X.-L.; Xu, N.; Cheng, H.-M.; et al. Tailoring the thermal and electrical transport properties of graphene films by grain size engineering. *Nat. Commun.* **2017**, *8*, 14486. [CrossRef] [PubMed]
24. Xin, G.; Zhu, W.; Yao, T.; Scott, S.M.; Lian, J. Microstructure control of macroscopic graphene paper by electrospray deposition and its effect on thermal and electrical conductivities. *Appl. Phys. Lett.* **2017**, *110*, 091909. [CrossRef]
25. Gee, C.M.; Tseng, C.C.; Wu, F.Y.; Lin, C.T.; Chang, H.P.; Li, L.J.; Chen, J.C.; Hu, L.H. Few layer graphene paper from electrochemical process for heat conduction. *Mater. Res. Innov.* **2014**, *18*, 208–213. [CrossRef]
26. Yu, W.; Xie, H.; Li, F.; Zhao, J.; Zhang, Z. Significant thermal conductivity enhancement in graphene oxide papers modified with alkaline earth metal ions. *Appl. Phys. Lett.* **2013**, *103*, 141913. [CrossRef]
27. Kong, Q.-Q.; Liu, Z.; Gao, J.-G.; Chen, C.-M.; Zhang, Q.; Zhou, G.; Tao, Z.-C.; Zhang, X.-H.; Wang, M.-Z.; Li, F.; et al. Hierarchical graphene–carbon fiber composite paper as a flexible lateral heat spreader. *Adv Funct. Mater.* **2014**, *24*, 4222–4228. [CrossRef]
28. Peng, L.; Xu, Z.; Liu, Z.; Guo, Y.; Li, P.; Gao, C. Ultrahigh thermal conductive yet superflexible graphene films. *Adv. Mater.* **2017**, *29*, 1700589. [CrossRef] [PubMed]
29. Weng, Z.; Su, Y.; Wang, D.-W.; Li, F.; Du, J.; Cheng, H.-M. Graphene–cellulose paper flexible supercapacitors. *Adv. Energy Mater.* **2011**, *1*, 917–922. [CrossRef]
30. Wan, S.; Li, Y.; Peng, J.; Hu, H.; Cheng, Q.; Jiang, L. Synergistic toughening of graphene oxide–molybdenum disulfide–thermoplastic polyurethane ternary artificial nacre. *ACS Nano* **2015**, *9*, 708–714. [CrossRef] [PubMed]
31. Hou, Z.-L.; Song, W.-L.; Wang, P.; Meziani, M.J.; Kong, C.Y.; Anderson, A.; Maimaiti, H.; LeCroy, G.E.; Qian, H.; Sun, Y.-P. Flexible graphene–graphene composites of superior thermal and electrical transport properties. *ACS Appl. Mater. Interfaces* **2014**, *6*, 15026–15032. [CrossRef] [PubMed]
32. Huang, W.; Ouyang, X.; Lee, L.J. High-performance nanopapers based on benzenesulfonic functionalized graphenes. *ACS Nano* **2012**, *6*, 10178–10185. [CrossRef] [PubMed]
33. Zhang, Y.; Han, H.; Wang, N.; Zhang, P.; Fu, Y.; Murugesan, M.; Edwards, M.; Jeppson, K.; Volz, S.; Liu, J. Improved heat spreading performance of functionalized graphene in microelectronic device application. *Adv. Funct. Mater.* **2015**, *25*, 4430–4435. [CrossRef]
34. Teng, C.; Xie, D.; Wang, J.; Yang, Z.; Ren, G.; Zhu, Y. Ultrahigh conductive graphene paper based on ball-milling exfoliated graphene. *Adv. Funct. Mater.* **2017**, *27*, 1700240. [CrossRef]
35. Wu, H.; Drzal, L.T. Graphene nanoplatelet paper as a light-weight composite with excellent electrical and thermal conductivity and good gas barrier properties. *Carbon* **2012**, *50*, 1135–1145. [CrossRef]
36. Kumar, P.; Shahzad, F.; Yu, S.; Hong, S.M.; Kim, Y.-H.; Koo, C.M. Large-area reduced graphene oxide thin film with excellent thermal conductivity and electromagnetic interference shielding effectiveness. *Carbon* **2015**, *94*, 494–500. [CrossRef]
37. Shen, B.; Zhai, W.; Zheng, W. Ultrathin flexible graphene film: An excellent thermal conducting material with efficient EMI shielding. *Adv. Funct. Mater.* **2014**, *24*, 4542–4548. [CrossRef]
38. Renteria, J.D.; Ramirez, S.; Malekpour, H.; Alonso, B.; Centeno, A.; Zurutuza, A.; Cocemasov, A.I.; Nika, D.L.; Balandin, A.A. Strongly anisotropic thermal conductivity of free-standing reduced graphene oxide films annealed at high temperature. *Adv. Funct. Mater.* **2015**, *25*, 4664–4672. [CrossRef]
39. Chen, C.; Yang, Q.-H.; Yang, Y.; Lv, W.; Wen, Y.; Hou, P.-X.; Wang, M.; Cheng, H.-M. Self-assembled free-standing graphite oxide membrane. *Adv. Mater.* **2009**, *21*, 3007–3011. [CrossRef]
40. Xin, G.; Sun, H.; Hu, T.; Fard, H.R.; Sun, X.; Koratkar, N.; Borca-Tasciuc, T.; Lian, J. Large-area freestanding graphene paper for superior thermal management. *Adv. Mater.* **2014**, *26*, 4521–4526. [CrossRef] [PubMed]
41. Zhu, Y.; Murali, S.; Cai, W.; Li, X.; Suk, J.W.; Potts, J.R.; Ruoff, R.S. Graphene and graphene oxide: Synthesis, properties, and applications. *Adv. Mater.* **2010**, *22*, 3906–3924. [CrossRef] [PubMed]

42. Huang, S.-Y.; Zhao, B.; Zhang, K.; Yuen, M.M.F.; Xu, J.-B.; Fu, X.-Z.; Sun, R.; Wong, C.-P. Enhanced reduction of graphene oxide on recyclable cu foils to fabricate graphene films with superior thermal conductivity. *Sci. Rep.* **2015**, *5*, 14260. [CrossRef] [PubMed]
43. Fan, Z.; Marconnet, A.; Nguyen, S.T.; Lim, C.Y.H.; Duong, H.M. Effects of heat treatment on the thermal properties of highly nanoporous graphene aerogels using the infrared microscopy technique. *Int. J. Heat Mass Transf.* **2014**, *76*, 122–127. [CrossRef]
44. Fan, Z.; Tng, D.Z.Y.; Lim, C.X.T.; Liu, P.; Nguyen, S.T.; Xiao, P.; Marconnet, A.; Lim, C.Y.H.; Duong, H.M. Thermal and electrical properties of graphene/carbon nanotube aerogels. *Colloids Surf. A Physicochem. Eng. Asp.* **2014**, *445*, 48–53. [CrossRef]
45. Fan, Z.; Tng, D.Z.Y.; Nguyen, S.T.; Feng, J.D.; Lin, C.F.; Xiao, P.F.; Lu, L.; Duong, H.M. Morphology effects on electrical and thermal properties of binderless graphene aerogels. *Chem. Phys. Lett.* **2013**, *561*, 92–96. [CrossRef]
46. Li, A.; Zhang, C.; Zhang, Y.-F. Thermal conductivities of PU composites with graphene aerogels reduced by different methods. *Compos. Part A Appl. Sci. Manuf.* **2017**, *103*, 161–167. [CrossRef]
47. Yang, W.; Zhao, Z.; Wu, K.; Huang, R.; Liu, T.; Jiang, H.; Chen, F.; Fu, Q. Ultrathin flexible reduced graphene oxide/cellulose nanofiber composite films with strongly anisotropic thermal conductivity and efficient electromagnetic interference shielding. *J. Mater. Chem. C* **2017**, *5*, 3748–3756. [CrossRef]
48. Jin, S.; Gao, Q.; Zeng, X.; Zhang, R.; Liu, K.; Shao, X.; Jin, M. Effects of reduction methods on the structure and thermal conductivity of free-standing reduced graphene oxide films. *Diam. Relat. Mater.* **2015**, *58*, 54–61. [CrossRef]
49. Pham, V.H.; Cuong, T.V.; Hur, S.H.; Shin, E.W.; Kim, J.S.; Chung, J.S.; Kim, E.J. Fast and simple fabrication of a large transparent chemically-converted graphene film by spray-coating. *Carbon* **2010**, *48*, 1945–1951. [CrossRef]
50. Gilje, S.; Han, S.; Wang, M.; Wang, K.L.; Kaner, R.B. A chemical route to graphene for device applications. *Nano Lett.* **2007**, *7*, 3394–3398. [CrossRef] [PubMed]
51. Zhao, J.; Pei, S.; Ren, W.; Gao, L.; Cheng, H.-M. Efficient preparation of large-area graphene oxide sheets for transparent conductive films. *ACS Nano* **2010**, *4*, 5245–5252. [CrossRef] [PubMed]
52. Wu, J.; Becerril, H.A.; Bao, Z.; Liu, Z.; Chen, Y.; Peumans, P. Organic solar cells with solution-processed graphene transparent electrodes. *Appl. Phys. Lett.* **2008**, *92*, 263302. [CrossRef]
53. Polsen, E.S.; McNerny, D.Q.; Viswanath, B.; Pattinson, S.W.; Hart, A.J. High-speed roll-to-roll manufacturing of graphene using a concentric tube CVD reactor. *Sci. Rep.* **2015**, *5*, 10257. [CrossRef] [PubMed]
54. Hu, D.; Gong, W.; Di, J.; Li, D.; Li, R.; Lu, W.; Gu, B.; Sun, B.; Li, Q. Strong graphene-interlayered carbon nanotube films with high thermal conductivity. *Carbon* **2017**, *118*, 659–665. [CrossRef]
55. Novoselov, K.S.; Falko, V.I.; Colombo, L.; Gellert, P.R.; Schwab, M.G.; Kim, K. A roadmap for graphene. *Nature* **2012**, *490*, 192–200. [CrossRef] [PubMed]
56. Yang, J.; Qi, G.-Q.; Liu, Y.; Bao, R.-Y.; Liu, Z.-Y.; Yang, W.; Xie, B.-H.; Yang, M.-B. Hybrid graphene aerogels/phase change material composites: Thermal conductivity, shape-stabilization and light-to-thermal energy storage. *Carbon* **2016**, *100*, 693–702. [CrossRef]
57. Balandin, A.A. Thermal properties of graphene and nanostructured carbon materials. *Nat. Mater.* **2011**, *10*, 569–581. [CrossRef] [PubMed]
58. Balandin, A.A.; Ghosh, S.; Bao, W.; Calizo, I.; Teweldebrhan, D.; Miao, F.; Lau, C.N. Superior thermal conductivity of single-layer graphene. *Nano Lett.* **2008**, *8*, 902–907. [CrossRef] [PubMed]
59. Banszerus, L.; Schmitz, M.; Engels, S.; Goldsche, M.; Watanabe, K.; Taniguchi, T.; Beschoten, B.; Stampfer, C. Ballistic transport exceeding 28 μm in CVD grown graphene. *Nano Lett.* **2015**, *16*, 1387. [CrossRef] [PubMed]
60. Fugallo, G.; Cepellotti, A.; Paulatto, L.; Lazzeri, M.; Marzari, N.; Mauri, F. Thermal conductivity of graphene and graphite: Collective excitations and mean free paths. *Nano Lett.* **2014**, *14*, 6109–6114. [CrossRef] [PubMed]
61. Ding, J.; ur Rahman, O.; Zhao, H.; Peng, W.; Dou, H.; Chen, H.; Yu, H. Hydroxylated graphene-based flexible carbon film with ultrahigh electrical and thermal conductivity. *Nanotechnology* **2017**, *28*, 39LT01. [CrossRef] [PubMed]
62. Song, N.-J.; Chen, C.-M.; Lu, C.; Liu, Z.; Kong, Q.-Q.; Cai, R. Thermally reduced graphene oxide films as flexible lateral heat spreaders. *J. Mater. Chem. A* **2014**, *2*, 16563–16568. [CrossRef]

63. Huang, Y.; Gong, Q.; Zhang, Q.; Shao, Y.; Wang, J.; Jiang, Y.; Zhao, M.; Zhuang, D.; Liang, J. Fabrication and molecular dynamics analyses of highly thermal conductive reduced graphene oxide films at ultra-high temperatures. *Nanoscale* **2017**, *9*, 2340–2347. [CrossRef] [PubMed]
64. Liu, S.Q.; Zhang, K.; Yuen, M.M.F.; Fu, X.Z.; Sun, R.; Wong, C.P. Effect of reduction temperatures on the thermal and electrical conductivities of reduced graphene oxide films on the CU foils. In Proceedings of the 2016 17th International Conference on Electronic Packaging Technology (ICEPT), Guangzhou, China, 16–19 August 2016; pp. 310–312.
65. Pop, E.; Varshney, V.; Roy, A.K. Thermal properties of graphene: Fundamentals and applications. *MRS Bull.* **2012**, *37*, 1273–1281. [CrossRef]
66. Ng, T.Y.; Yeo, J.J.; Liu, Z.S. A molecular dynamics study of the thermal conductivity of graphene nanoribbons containing dispersed stone–thrower–wales defects. *Carbon* **2012**, *50*, 4887–4893. [CrossRef]
67. Cui, L.; Du, X.; Wei, G.; Feng, Y. Thermal conductivity of graphene wrinkles: A molecular dynamics simulation. *J. Phys. Chem. C* **2016**, *120*, 23807–23812. [CrossRef]
68. Xu, W.; Zhang, G.; Li, B. Thermal conductivity of penta-graphene from molecular dynamics study. *J. Chem. Phys.* **2015**, *143*, 154703. [CrossRef] [PubMed]
69. Shtein, M.; Nadiv, R.; Buzaglo, M.; Kahil, K.; Regev, O. Thermally conductive graphene-polymer composites: Size, percolation, and synergy effects. *Chem. Mater.* **2015**, *27*, 2100–2106. [CrossRef]
70. Song, W.-L.; Cao, M.-S.; Lu, M.-M.; Bi, S.; Wang, C.-Y.; Liu, J.; Yuan, J.; Fan, L.-Z. Flexible graphene/polymer composite films in sandwich structures for effective electromagnetic interference shielding. *Carbon* **2014**, *66*, 67–76. [CrossRef]
71. Kumar, P.; Kumar, A.; Cho, K.Y.; Das, T.K.; Sudarsan, V. An asymmetric electrically conducting self-aligned graphene/polymer composite thin film for efficient electromagnetic interference shielding. *AIP Adv.* **2017**, *7*, 015103. [CrossRef]
72. Rahim, J.; Amir, H.; Muhammad Aftab, A.; Imtiaz, A.; Attaullah, S.; Muhammad, S.; Akhtar, H. Flexible, thin films of graphene–polymer composites for emi shielding. *Mater. Res. Express* **2017**, *4*, 035605.
73. Wang, B.; Zhang, Y.; Zhang, J.; Xia, R.; Chu, Y.; Zhou, J.; Yang, X.; Huang, J. Facile synthesis of a MoS_2 and functionalized graphene heterostructure for enhanced lithium-storage performance. *ACS Appl. Mater. Interfaces* **2017**, *9*, 12907–12913. [CrossRef] [PubMed]
74. Fang, Y.; Lv, Y.; Gong, F.; Elzatahry, A.A.; Zheng, G.; Zhao, D. Synthesis of 2D-mesoporous-carbon/ MoS_2 heterostructures with well-defined interfaces for high-performance lithium-ion batteries. *Adv. Mater.* **2016**, *28*, 9385–9390. [CrossRef] [PubMed]
75. Teng, Y.; Zhao, H.; Zhang, Z.; Li, Z.; Xia, Q.; Zhang, Y.; Zhao, L.; Du, X.; Du, Z.; Lv, P.; et al. MoS_2 nanosheets vertically grown on graphene sheets for lithium-ion battery anodes. *ACS Nano* **2016**, *10*, 8526–8535. [CrossRef] [PubMed]
76. Gong, F.; Papavassiliou, D.V.; Duong, H.M. Off-lattice monte carlo simulation of heat transfer through carbon nanotube multiphase systems taking into account thermal boundary resistances. *Numer. Heat Transf. Part A Appl.* **2014**, *65*, 1023–1043. [CrossRef]
77. Gong, F.; Duong, H.M.; Papavassiliou, D.V. Inter-carbon nanotube contact and thermal resistances in heat transport of three-phase composites. *J. Phys. Chem. C* **2015**, *119*, 7614–7620. [CrossRef]
78. Eslami, H.; Mohammadzadeh, L.; Mehdipour, N. Reverse nonequilibrium molecular dynamics simulation of thermal conductivity in nanoconfined polyamide-6,6. *J. Chem. Phys.* **2011**, *135*, 064703. [CrossRef] [PubMed]
79. Eslami, H.; Mohammadzadeh, L.; Mehdipour, N. Anisotropic heat transport in nanoconfined polyamide-6,6 oligomers: Atomistic reverse nonequilibrium molecular dynamics simulation. *J. Chem. Phys.* **2012**, *136*, 104901. [CrossRef] [PubMed]
80. Eslami, H.; Mehdipour, F.; Setoodeh, A.; Rouzegar, J. Nanoconfined polymers: Modelling and simulation approaches. *Mol. Simul.* **2015**, *41*, 367–381. [CrossRef]
81. Gao, Y.; Müller-Plathe, F. Increasing the thermal conductivity of graphene-polyamide-6,6 nanocomposites by surface-grafted polymer chains: Calculation with molecular dynamics and effective-medium approximation. *J. Phys. Chem. B* **2016**, *120*, 1336–1346. [CrossRef] [PubMed]
82. Marconnet, A.M.; Ashegi, M.; Goodson, K.E. From the casimir limit to phononic crystals: 20 years of phonon transport studies using silicon-on-insulator technology. *J. Heat Transf.* **2013**, *135*, 061601. [CrossRef]
83. Marconnet, A.M.; Panzer, M.A.; Goodson, K.E. Thermal conduction phenomena in carbon nanotubes and related nanostructured materials. *Rev. Mod. Phys.* **2013**, *85*, 1295–1326. [CrossRef]

84. Gong, F.; Liu, J.; Yang, J.; Qin, J.; Yang, Y.; Feng, T.; Liu, W.; Duong, H.; Papavassiliou, D.V.; Wu, M. Effective thermal transport properties in multiphase biological systems containing carbon nanomaterials. *RSC Adv.* **2017**, *7*, 13615–13622. [CrossRef]
85. Lin, S.C.; Buehler, M.J. The effect of non-covalent functionalization on the thermal conductance of graphene/organic interfaces. *Nanotechnology* **2013**, *24*, 165702. [CrossRef] [PubMed]
86. Zhao, W.; Kong, J.; Liu, H.; Zhuang, Q.; Gu, J.; Guo, Z. Ultra-high thermally conductive and rapid heat responsive poly(benzobisoxazole) nanocomposites with self-aligned graphene. *Nanoscale* **2016**, *8*, 19984–19993. [CrossRef] [PubMed]
87. Yao, Y.; Zeng, X.; Wang, F.; Sun, R.; Xu, J.-B.; Wong, C.-P. Significant enhancement of thermal conductivity in bioinspired freestanding boron nitride papers filled with graphene oxide. *Chem. Mater.* **2016**, *28*, 1049–1057. [CrossRef]
88. Zhang, X.; Zhang, X.; Yang, M.; Yang, S.; Wu, H.; Guo, S.; Wang, Y. Ordered multilayer film of (graphene oxide/polymer and boron nitride/polymer) nanocomposites: An ideal emi shielding material with excellent electrical insulation and high thermal conductivity. *Compos. Sci. Technol.* **2016**, *136*, 104–110. [CrossRef]
89. Song, N.; Jiao, D.; Ding, P.; Cui, S.; Tang, S.; Shi, L. Anisotropic thermally conductive flexible films based on nanofibrillated cellulose and aligned graphene nanosheets. *J. Mater. Chem. C* **2016**, *4*, 305–314. [CrossRef]
90. Gong, J.; Liu, Z.; Yu, J.; Dai, D.; Dai, W.; Du, S.; Li, C.; Jiang, N.; Zhan, Z.; Lin, C.-T. Graphene woven fabric-reinforced polyimide films with enhanced and anisotropic thermal conductivity. *Compos. Part A Appl. Sci. Manuf.* **2016**, *87*, 290–296. [CrossRef]
91. George, G.; Sisupal, S.B.; Tomy, T.; Pottammal, B.A.; Kumaran, A.; Suvekbala, V.; Gopimohan, R.; Sivaram, S.; Ragupathy, L. Thermally conductive thin films derived from defect free graphene-natural rubber latex nanocomposite: Preparation and properties. *Carbon* **2017**, *119*, 527–534. [CrossRef] [PubMed]
92. Hwang, Y.; Kim, M.; Kim, J. Enhancement of thermal and mechanical properties of flexible graphene oxide/carbon nanotube hybrid films though direct covalent bonding. *J. Mater. Sci.* **2013**, *48*, 7011–7021. [CrossRef]
93. Yu, A.; Roes, I.; Davies, A.; Chen, Z. Ultrathin, transparent, and flexible graphene films for supercapacitor application. *Appl. Phys. Lett.* **2010**, *96*, 253105. [CrossRef]
94. Obreja, A.C.; Iordanescu, S.; Gavrila, R.; Dinescu, A.; Comanescu, F.; Matei, A.; Danila, M.; Dragoman, M.; Iovu, H. Flexible films based on graphene/polymer nanocomposite with improved electromagnetic interference shielding. In Proceedings of the 2015 International Semiconductor Conference (CAS), Sinaia, Romania, 12–14 October 2015; pp. 49–52.
95. Indrani, B.; Tsegie, F.; Zlatka, S.; Paul, G.H.; Chen, J.; Ashwani, K.S.; Asim, K.R. Graphene films printable on flexible substrates for sensor applications. *2D Mater.* **2017**, *4*, 015036.
96. Pierleoni, D.; Xia, Z.Y.; Christian, M.; Ligi, S.; Minelli, M.; Morandi, V.; Doghieri, F.; Palermo, V. Graphene-based coatings on polymer films for gas barrier applications. *Carbon* **2016**, *96*, 503–512. [CrossRef]
97. Veronese, G.P.; Allegrezza, M.; Canino, M.; Centurioni, E.; Ortolani, L.; Rizzoli, R.; Morandi, V.; Summonte, C. Graphene as transparent conducting layer for high temperature thin film device applications. *Sol. Energy Mater. Sol. Cells* **2015**, *138*, 35–40. [CrossRef]
98. Song, W.; Kim, K.W.; Chang, S.-J.; Park, T.J.; Kim, S.H.; Jung, M.W.; Lee, G.; Myung, S.; Lim, J.; Lee, S.S.; et al. Direct growth of graphene nanopatches on graphene sheets for highly conductive thin film applications. *J. Mater. Chem. C* **2015**, *3*, 725–728. [CrossRef]
99. Anandan, S.; Narasinga Rao, T.; Sathish, M.; Rangappa, D.; Honma, I.; Miyauchi, M. Superhydrophilic graphene-loaded tio2 thin film for self-cleaning applications. *ACS Appl. Mater. Interfaces* **2013**, *5*, 207–212. [CrossRef] [PubMed]
100. Mosciatti, T.; Haar, S.; Liscio, F.; Ciesielski, A.; Orgiu, E.; Samorì, P. A multifunctional polymer-graphene thin-film transistor with tunable transport regimes. *ACS Nano* **2015**, *9*, 2357–2367. [CrossRef] [PubMed]